CONSTRAINING SOURCE TERMS, REGIONAL ATTENUATION MODELS, AND SITE EFFECTS

Mark D. Fisk[1] and W. Scott Phillips[2]

Alliant Techsystems[1] and Los Alamos National Laboratory[2]

Sponsored by Air Force Research Laboratory[1] and National Nuclear Security Administration[2]

Contract Nos. FA8718-09-C-0005[1] and LA09-BAA09-01-NDD03[2]

ABSTRACT

This effort is directed at improving the calibration of Q, geometrical spreading, source, and site effects for regional seismic phases in Eurasia. As a starting point, we have used spectral ratios of regional phases for nearby similar earthquakes of different moments to eliminate path and site effects, giving more reliable estimates of source parameters. We then correct the spectra for the source terms to estimate more reliable distance and site terms. As shown by Schaff and Richards (2004) and Fisk et al. (2007), there are many such pairs of events throughout Eurasia available for this Empirical Green's Function (EGF) analysis. In addition, a key element of this effort has been to incorporate coda envelope measurements in a suite of frequency bands, using the method as Mayeda et al. (2003) and Phillips et al. (2008). We compute a pseudo relative spectrum as the median ratio of coda envelopes in 16 frequency bands, which does not require the usual coda calibration. As shown by Mayeda et al. (2007), coda is less sensitive to focal mechanism, event separation, and station coverage. Spectra of direct phases and coda envelopes each have distinct advantages; the independence of the methods and portions of the waveforms measured corroborates the estimated source terms or, in cases of discrepancies, helps identify problems. We have processed a large dataset of three-component regional seismograms from IRIS for events listed in the PDE from 1989 to 2009. We have processed and fit a relative Brune (1970) source model to network-median relative spectra for over 46,000 pairs, corresponding to about 9,400 unique events. We have reviewed and selected results with good corroboration of the moments and corner frequencies from coda and direct phases. More recently, we have been fitting source-corrected spectra to estimate Q effects and comparing the results to those of amplitude tomography work at Los Alamos National Laboratory (LANL). These are orthogonal/independent approaches in the sense that the spectral fits estimate the frequency dependence of Q for fixed paths, while the tomography analysis estimates the path dependence of Q for 12 fixed frequency bands. There is generally good agreement of Lg Q estimates from the two methods for areas with good station coverage. We show comparisons of the results for all of the paths processed thus far and highlight some representative cases in more detail. We have also investigated discrepancies in the Q estimates, typically for higher frequencies, in low Q regions, and/or at the edges of the tomography grid. Most of the discrepancies can be attributed to stations with strong site effects (that impact Q estimates from fitting source-corrected spectra), grid resolution/edge effects and data quality issues in higher frequency bands (that impact tomography results). We show how site terms estimated from coda tomography, independent of both the direct Lg amplitude tomography and fitting of source-corrected spectra, as well as improvements in data quality for tomography, resolve significant discrepancies (e.g., for station KMI in China), leading to results that converge to the same answer. We are working to merge the estimated source terms and Q results as constraints on the tomography analysis. We are also extending this analysis and the comparisons to other regional phases.

OBJECTIVES

We are developing, applying, and evaluating methods to improve the accuracy of attenuation models, geometrical spreading, site terms, and their uncertainties for regional phases in Eurasia, by constraining trade-offs among the parameters at various stages of the analysis. The approach is to break up traditional grid-search inversions, which are known to have many trade-offs and instabilities, into manageable pieces, canceling out certain physical effects (e.g., distance and site) to allow reliable estimation of others (e.g., source), and then correcting for the latter to then estimate reliable parameters for the former. We are processing spectra of direct phases and coda envelope measurements to augment and corroborate source terms, and to independently estimate site terms. To validate the results, we are also using independent methods and data to estimate Q parameters. We plan to quantify the uncertainties and their correlation lengths, interpolate grids of stress drop, geometrical spreading, and Q estimates, and merge our results with amplitude tomography developments at LANL. We plan to evaluate the corrections and uncertainties using two large datasets and cross-validation methods.

RESEARCH ACCOMPLISHED

Following Sereno et al. (1988), Taylor and Hartse (1998), Taylor et al. (2002), and numerous others, the amplitude spectrum for a given phase and station, for event *i*, is modeled by

$$A_i(f) = S_i(f;M_0, f_c)G(r_i;r_0,\eta)\exp\left(-\frac{\pi f^{1-\gamma}}{Q_0 \nu} r_i\right)P(f), \quad \text{(EQ 1)}$$

where $S_i(f)$ is the source spectrum with moment M_0 (and radiation pattern terms) and corner frequency f_c, r_i is epicentral distance, $P(f)$ is a frequency-dependent site term, $Q_0 f^{\gamma}$ represents anelastic attenuation, ν is group velocity, and $G(r_i;r_0,\eta)$ represents frequency-independent geometrical spreading, inversely proportional to distance to a power η, beyond a reference distance r_0.

Estimating Source Terms

Rather than inverting for all parameters simultaneously, we start by using relative spectra for event pairs with similar locations and focal mechanisms (assessed by waveform cross-correlations), but different moments, to factor out path and site effects and obtain reliable estimates of the source terms. Once accurate source terms are estimated, the source-corrected spectra can be used to estimate the distance and site terms. That is, for a pair of nearby earthquakes with similar radiation patterns, the relative spectra for a given seismic phase type is modeled (Brune, 1970) by

$$\frac{A_1(f)}{A_2(f)} = \frac{S_1(f)}{S_2(f)} = \frac{M_0^{(1)}[1 + (f/f_c{}^{(2)})^2]}{M_0^{(2)}[1 + (f/f_c{}^{(1)})^2]}. \quad \text{(EQ 2)}$$

This approach requires many similar pairs. Schaff and Richards (2004) showed that there are indeed many such pairs of repeating events. In addition, Mayeda et al. (2007) showed that coda is less sensitive to focal mechanism, event separation, and station coverage. This allows the requirement of similar events to be relaxed, augmenting the number of pairs for which source terms can be estimated. Thus, in addition to using relative spectra of direct regional phases, we compute coda envelopes, using the processing method as Mayeda et al. (2003) and Phillips et al. (2008). We then compute a pseudo relative spectrum as the median ratio of coda envelopes in 16 frequency bands. For example, Figure 1 shows relative spectra of Pn, Sn, Lg, and Lg coda, along with source model fits for an earthquake pair in southwestern Siberia. Note that the relative coda spectrum, just using MK31 three-component (3C) data, is nearly the same as the network results for coda and direct phases using 19 regional stations. The independence of direct-phase spectra and coda envelopes is used to corroborate the estimated source terms (moments and corner frequencies).

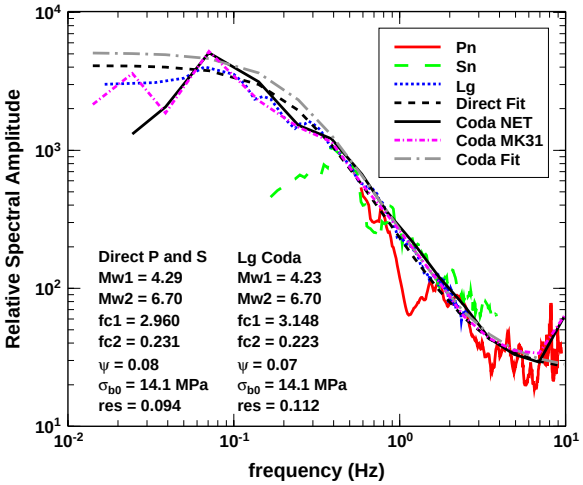

Figure 1. Network-median relative spectra of Pn, Sn, Lg, and Lg coda (using 19 stations and just MK31) for an event pair in southwestern Siberia. Model fits and estimated source parameters agree very well.

We acquired regional data from IRIS for events listed in PDE from 1989 to 2009 that have epicenter estimates within 50 km of another event, a magnitude difference of at least 0.7 m.u., and the larger event of each pair at least mb 5. The set includes 46,495 such pairs, corresponding to 9,395 unique events, shown in Figure 2. We processed about 2,000,000 spectra of regional phases and about 10,000,000 coda envelopes, computed network-median relative spectra, and fit Eq. (2) to each of the pairs. We also computed waveform cross-correlations for all pairs, to assess the similarity of mechanisms for cases where results from direct phases and coda disagree. We have reviewed the results for master events of $M_W \geq 5.4$, as well as smaller events for areas of interest. The bright markers in Figure 2 correspond to events with consistent source parameter estimates from coda and direct phases, as shown in Figure 3. The faint markers correspond to smaller processed pairs for which there are some useful results, but they have not been fully reviewed. Figure 2 also shows ray paths to IRIS stations with data for those events with corroborated source terms, indicating good coverage for much of Eurasia. Unlike tomography, this approach does not require crossing ray paths to estimate model parameters of Eq. (1), providing constraints for many paths and extending calibration to the edges of the grid (e.g., Russia, India, and the Arabian Peninsula). Because automatic processing is needed for this very large data set, to build confidence in the procedure and the resulting source terms, we compared coda and direct results in detail for many cases and to published results. Fisk and Phillips (2010) showed some that highlight the dependence of the results on station coverage and the benefits of using both direct phases and coda.

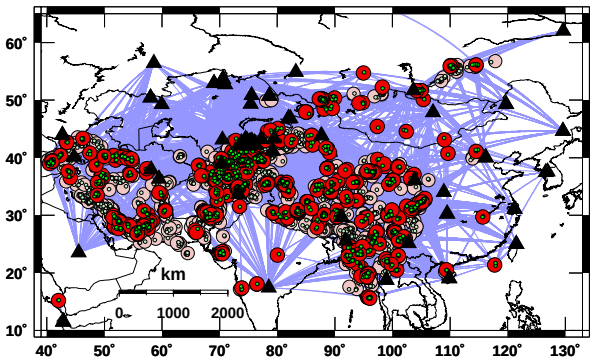

Figure 2. Map of earthquakes listed in the PDE from 1989 to 2009 for which we processed and fit relative spectra. Red circles correspond to larger events within 50 km of smaller events (green circles). Bright markers and ray paths are shown for events with consistent source terms from coda and direct phases.

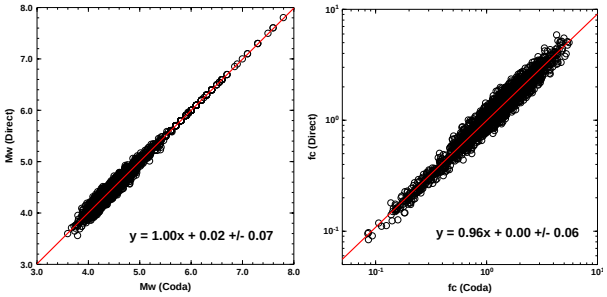

Figure 3. Comparisons of Mw (left) and corner-frequency (right) estimates from direct phases versus coda that are consistent. Moments of the large master events were fixed using values in the PDE; they were not used in the linear regression (left plot).

Estimating Distance and Site Terms

Given this large set of corroborated source terms, we have been fitting source-corrected spectra to estimate the distance and site terms, using the following equation for a given station/path and phase:

$$\log A(f)/S(f) \;=\; \log G + b + \log \varepsilon(f) - \frac{\pi f^{1-\gamma}}{Q_0 v} r \,,$$

where G is frequency-independent spreading, b is a constant site factor, $\varepsilon(f)$ represents the frequency

dependence of the site effect, and the last term represents attenuation. Note that G and b are constants with respect to frequency, while $Q(f) = Q_0 f^{\gamma}$ and $\varepsilon(f)$ represent the shape (i.e., frequency dependence) of the source-corrected spectra. Figure 4 illustrates source-corrected Lg (3C) spectra and the model fit at VOS for an event in eastern Kazakhstan. Fitting source-corrected spectra gives Q estimates as a function of frequency for fixed paths. This is an *orthogonal* approach to the amplitude tomography analysis at LANL, that estimates the path dependence of Q for fixed frequency bands. Thus, comparison of the results is intended to corroborate paths with reliable Q estimates and determine paths with discrepancies, for which Q needs to be improved.

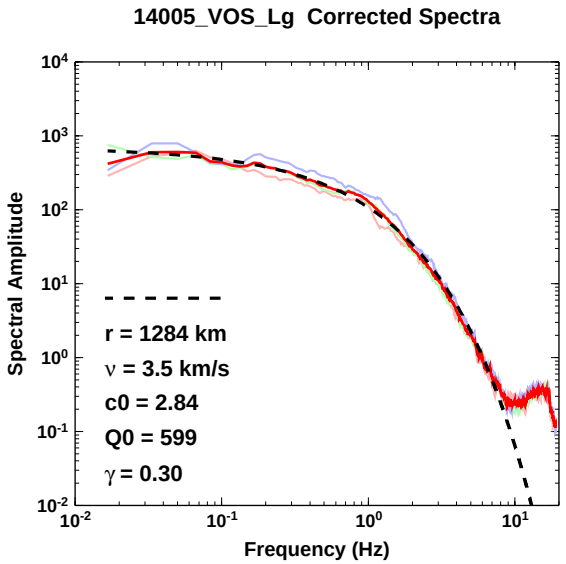

Figure 4. Source-corrected Lg spectra at station VOS for an earthquake in eastern Kazakhstan, the fit (dashed curve), and parameter estimates (legend).

To compare my Q_0 and γ estimates to the tomography results, the average of $Q(f)^{-1}$ was computed for each of 12 frequency bands, along each path shown in Figure 2. For each path, we then fit $\log Q(f) = \log Q_0 + \gamma \log f$ to the tomographic $Q(f)$ values to estimate Q_0 and γ, as illustrated by Figure 5 for Lg Q along the same path as Figure 4. For comparison, the red line is the result of spectral fitting from Figure 4, showing good agreement.

Figure 6 compares Lg Q results for one of the best cases, with good station coverage, corresponding to regional paths from an earthquake in the Tibetan Plateau. The Q_0 and γ estimates of the two methods agree very well (Figure 7). These are relatively low Q paths, particularly to stations LSA, KMI, and ENH, as expected for Lg propagation through the Tibetan Plateau. Figure 8 compares source-corrected Lg spectra and Q results of the two methods for KNET stations. We have found many other cases with excellent agreement, particularly in areas of good station coverage. Below we highlight some discrepancies and how the results of both methods can be improved.

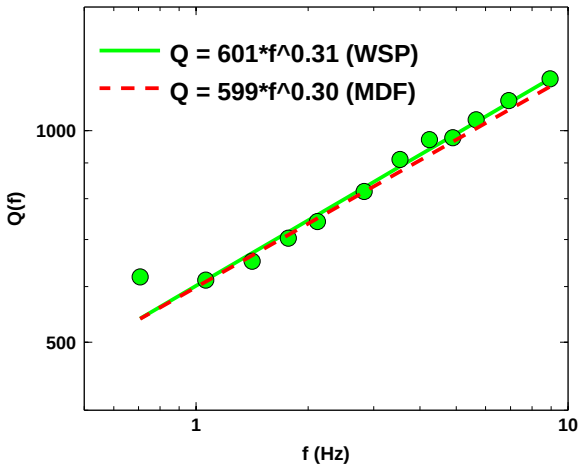

Figure 5. Comparison of Lg Q tomography results (green circles and line) to spectral fitting results (red line) for the path corresponding to Figure 4.

Figure 9 compares the Q_0 and γ estimates for all paths processed thus far, showing generally good agreement for Q_0, except for some outliers, while γ exhibits greater discrepancies, with higher estimates on average from tomography. It is useful to convert the effective Q estimates (illustrated by the color-coded rays in Figure 6) for this large set of paths into interpolated grids. We use a tomography code that inverts Q estimates for a suite of paths into a grid. (This is different from the amplitude tomography analysis that inverts amplitude data for Q grids.) Figure 10 (left) compares Lg Q grids at 1 Hz. As expected from Figure 9, they are quite similar, both showing relatively high Lg Q_0 for the Kazakhstan Platform, low values for the Tibetan Plateau, and intermediate values for eastern China. My spectral-fitting gives lower Q estimates in Iran and nearby areas, at the western edge of the amplitude-tomography grid. Figure 10 (right) compares Lg Q at 5 Hz, showing even lower Q estimates from my analysis than amplitude tomography for the Middle East.

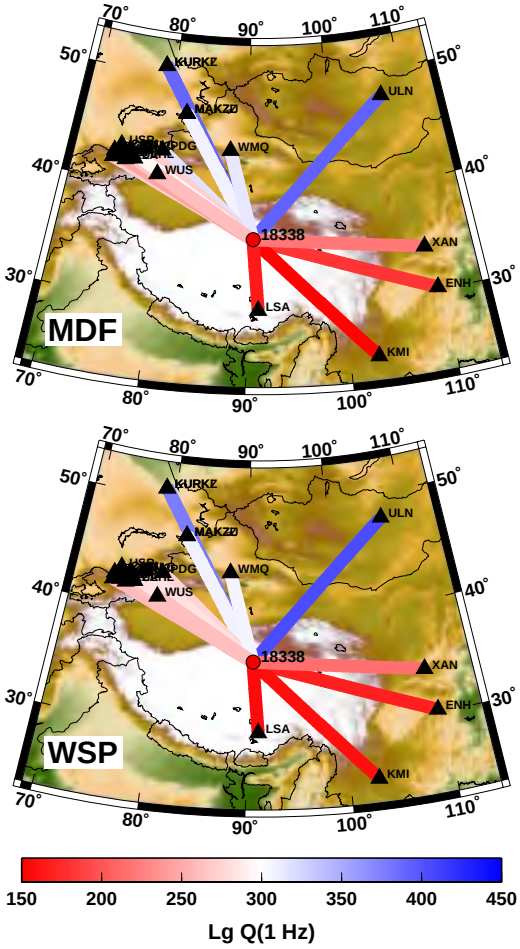

Figure 6. Comparison of effective Lg Q_0 estimates from fitting source-corrected spectra (top) and from amplitude tomography (bottom) for regional paths from an earthquake pair in the Tibetan Plateau.

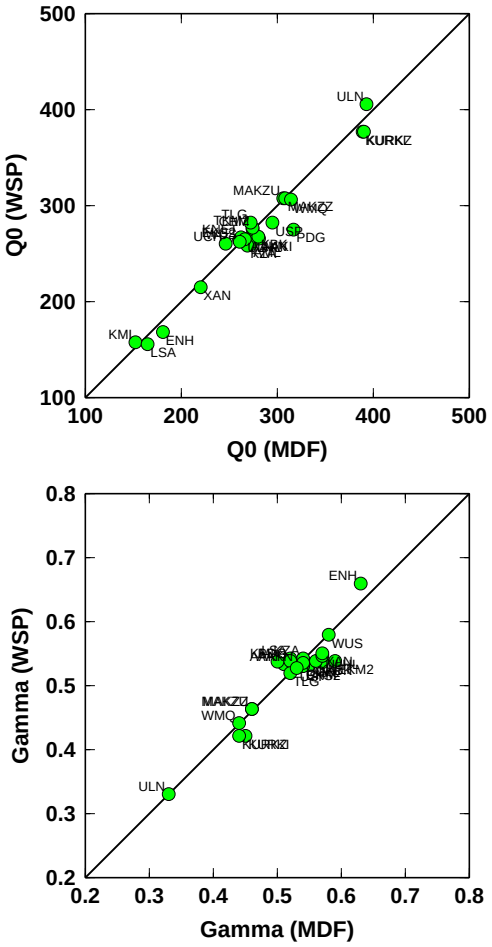

Figure 7. Direct comparison of Q_0 (top) and γ (bottom) estimates for the paths shown in Figure 6.

To understand the discrepancies in the γ estimates seen in Figure 9, Figure 11 provides detailed comparisons of the results at the western edge of the tomographic grid. The agreement is very good for some paths, (e.g., top plot of Figure 12), generally those with higher Q and better station coverage. For lower Q paths and worse coverage, the differences are progressively larger (e.g., bottom plot of Figure 12 for ABKT, which corresponds to one of the largest discrepancies in the γ estimates in Figure 9). Note for the bottom two plots that the lower bands of the tomography results (green circles) agree with the source-corrected spectra, but then deviate higher for the higher bands. These examples illustrate that fits of source-corrected spectra can improve and extend the amplitude-tomography grids at the edges.

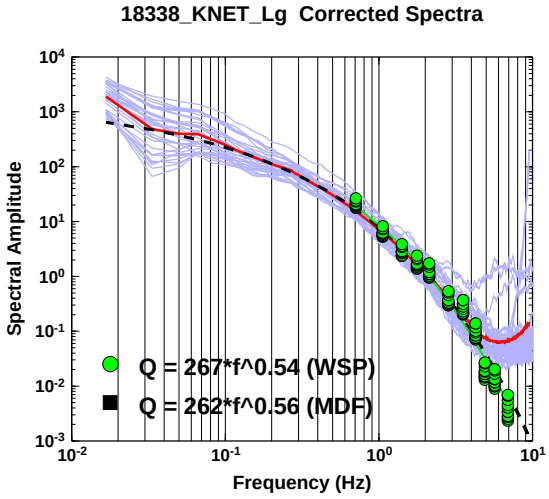

Figure 8. Source-corrected Lg spectra at KNET stations and comparison of Q parameter estimates for the Tibetan Plateau earthquakes.

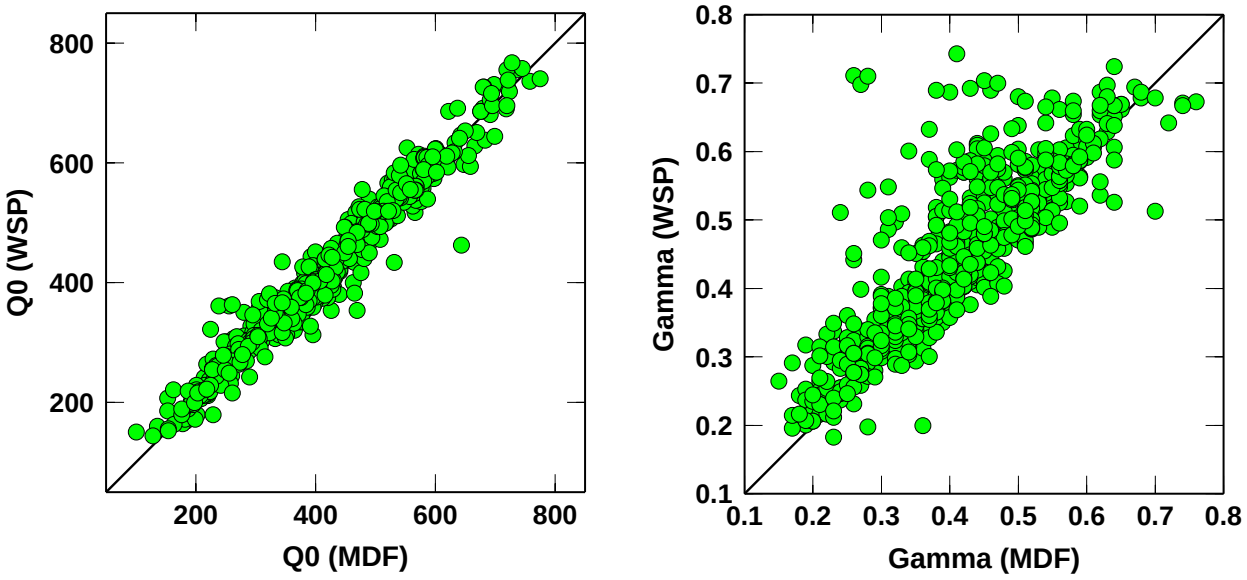

Figure 9. Comparison of Q_0 (left) and γ(right) estimates for all of the ray paths processed thus far.

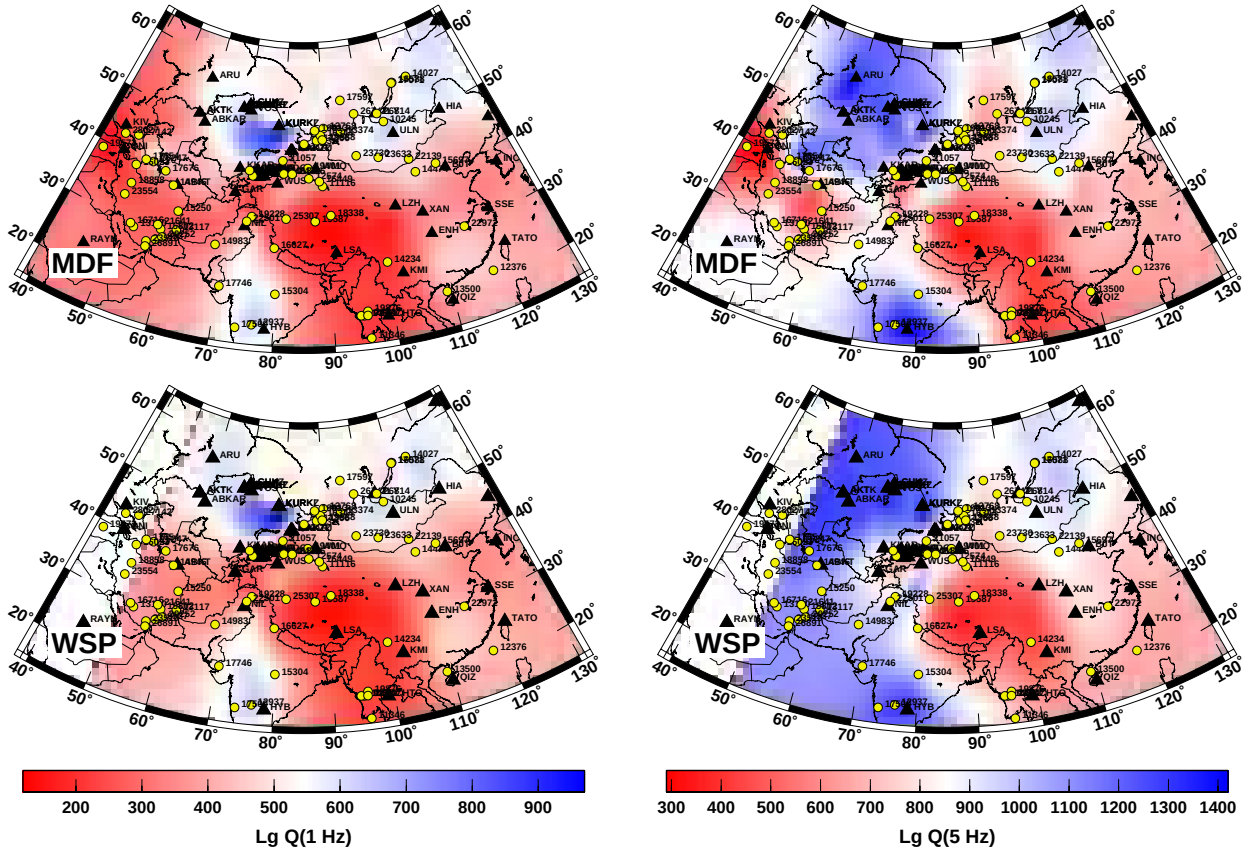

Figure 10. Comparison of Lg Q grids from spectral fitting (top) and amplitude tomography (bottom) at 1 Hz (left) and 5 Hz (right). The circles show events used in the analysis.

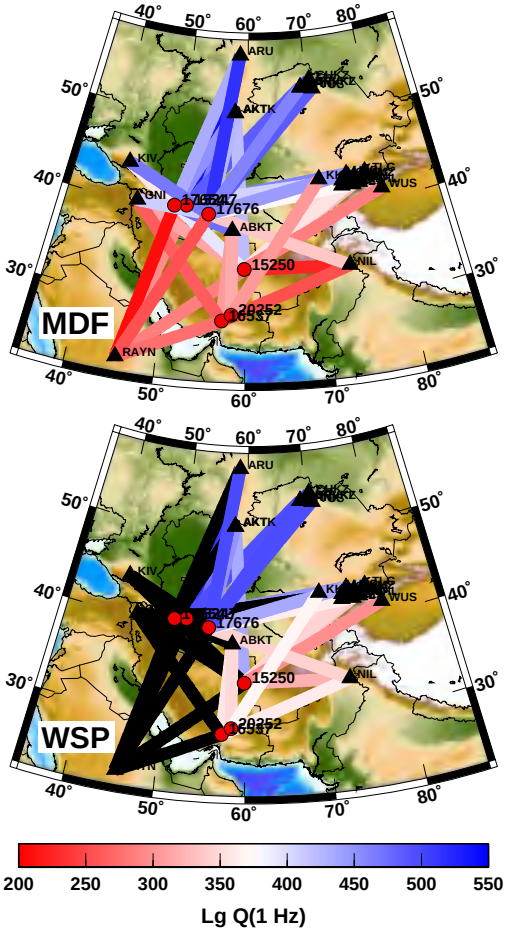

Figure 11. Comparison of Q_0 estimates for paths at the edge of the tomographic grid. Paths shown in black (lower map) are ones outside the tomographic grid, for which Q estimates are not available.

Site Effects

Some stations have strong frequency-dependent site effects. We have examined this to resolve some of the other larger discrepancies seen in Figure 9. Station KMI has some of the largest differences in γ estimates, as shown in the lower plot of Figure 13; the Q_0 estimates agree quite well. As an example, Figure 14 compares Q results for a path from Myanmar to KMI, which agree below 3 Hz, giving similar Q_0 estimates, but deviate at higher frequencies, leading to very different γ estimates. Figure 15 shows site terms for KMI computed from coda tomography, showing strong attenuation at frequencies greater than 1-2 Hz. Note also the difference in coda site terms for horizontal versus vertical channels. This behavior is also observed in the direct Lg spectra.

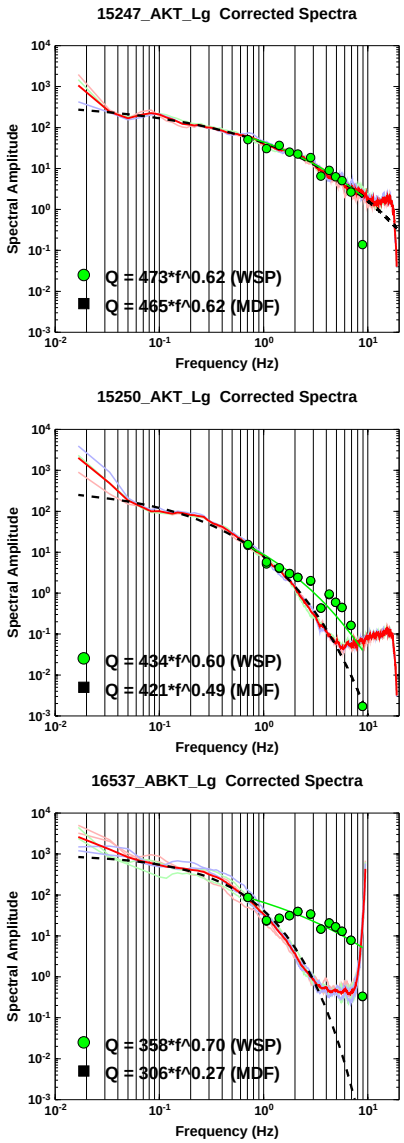

Figure 12. Comparisons spectral fits and tomography results for three of the paths shown in Figure 11.

Applying the coda site terms to the source-corrected Lg spectra and excluding the two highest bands in fitting tomographic $Q(f)$ estimates, yields the results shown in Figure 16. Thus, strong site attenuation is partially responsible for the different γ estimates, but poor data quality in the higher bands used for tomography is also a cause. Applying this analysis to all of the paths to KMI leads to results of the two methods that agree quite well. It is encouraging that proper treatment of these physical effects leads to results that converge to the same answer. We plan broad application of coda site terms to the source-corrected spectra, to improve the Q estimates.

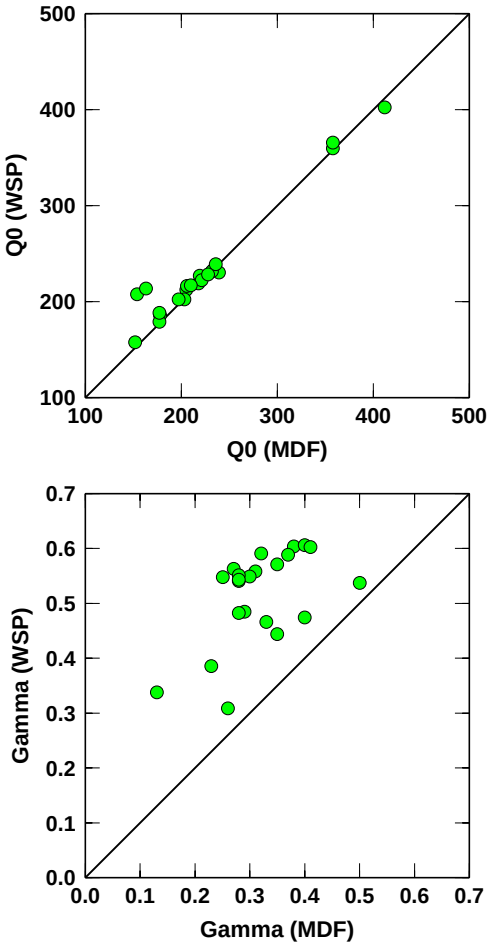

Figure 13. Comparison of Lg Q_0 (top) and γ (bottom) estimates for regional paths to station KMI.

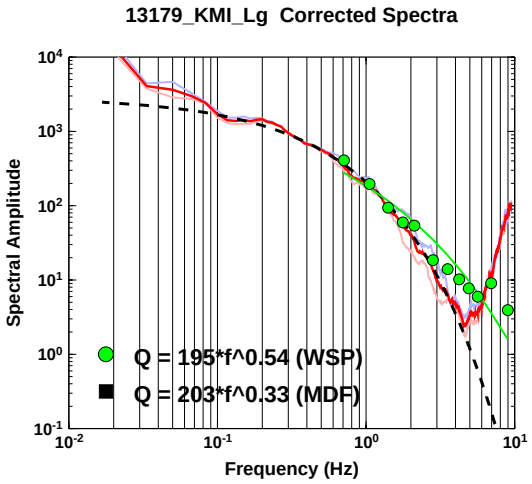

Figure 14. Source-corrected Lg spectra at KMI and *Q* results for an earthquake in Myanmar, which agree up to about 3 Hz, but deviate at higher frequencies.

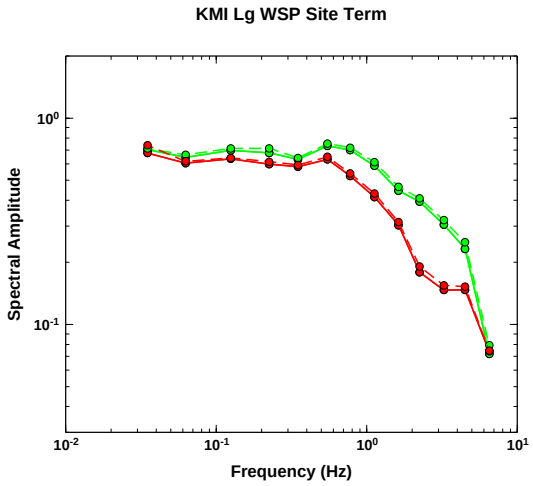

Figure 15. KMI site terms estimated from coda for various vertical and horizontal channels.

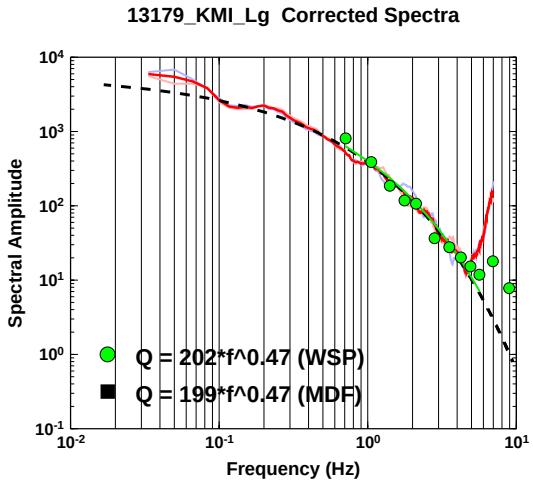

Figure 16. Similar to Figure 14, but correcting the source-corrected Lg spectra for site effects and excluding the two highest bands when regressing the tomographic *Q(f)* values to estimate Q_0 and γ

Application to Other Regional Phases

We have also started processing source-corrected Sn and Pn spectra. For example, Figure 17 compares my Sn Q estimates to those of tomography by Dr. Phillips. There is more scatter than for some of the best Lg comparisons (e.g., Figure 7), which is not surprising. Nevertheless, the results agree fairly well. Figure 18 shows the spectral comparison for KNET station EKS2.

Calibration of Pn Q is very important for regional P/S discrimination, especially using higher frequencies.

However, Pn is a very complicated and variable phase. Figure 19 shows source-corrected Pn spectra and Q comparisons for two paths to Kazakhstan Network (KZNET) stations BRVK, CHKZ, VOS, and ZRNK.

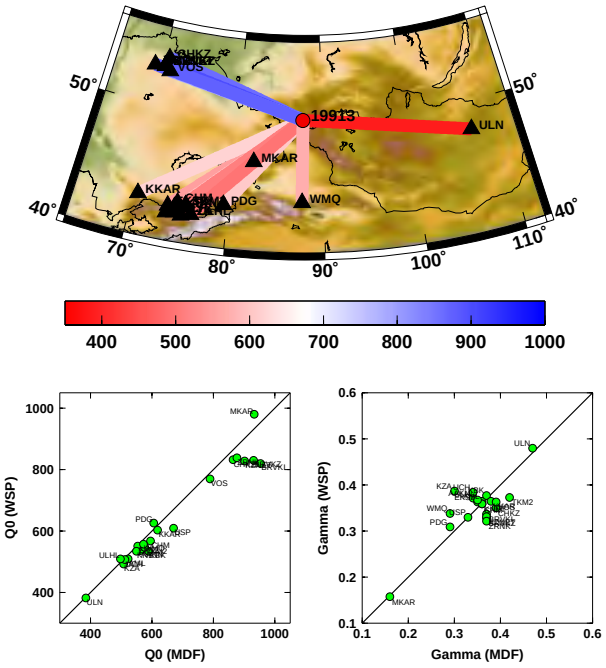

Figure 17. (top) Sn Q_0 estimates for regional paths from a cluster in southwestern Siberia; (bottom) comparison of Q_0 (left) and γ(right) estimates.

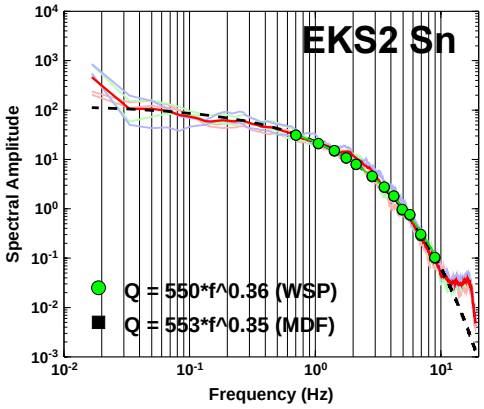

Figure 18. Comparison of a source-corrected Sn spectral fit to Sn Q estimates from tomography.

Orid 16449 was the Mw 5.5 earthquake on 30 January 1999 at the Lop Nor test site (LNTS). Orid 17597 was an Mw 5.5 earthquake in Russia, towards the northern part of the tomography grid, with more limited station coverage. Excluding the lowest and highest bands in regressing the tomography *Q(f)* values, the Q_0 and γ estimates from the two methods are similar for the path from LNTS. For the northern path, the Q_0 estimates agree, but the γ estimate from tomography is significantly higher. We plan to continue processing source-corrected Pn spectra to better constrain Pn Q.

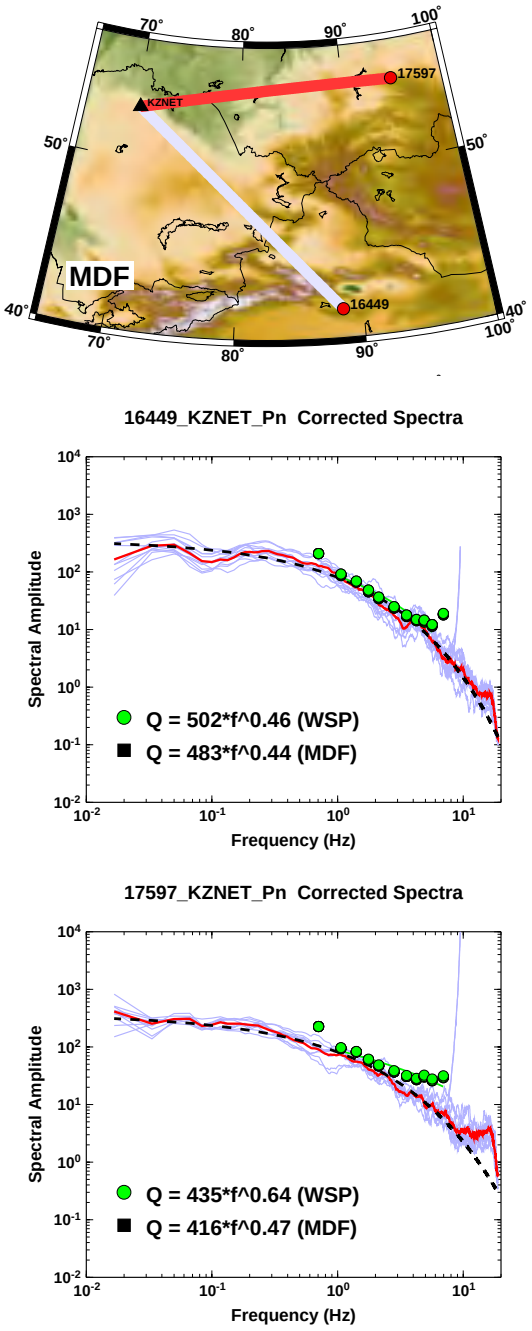

Figure 19. Examples of source-corrected Pn spectra and Q results for two paths to KZNET stations. The upper plot shows the results from LNTS. The lower plot shows the results for a northern path.

CONCLUSIONS AND RECOMMENDATIONS

We are developing and applying methods to improve the calibration of source, distance, and site corrections for regional seismic phases. We have processed 20 years of IRIS data for Eurasia. An important aspect has been to incorporate coda measurements to augment, corroborate, and improve source parameters estimated from relative spectra of direct phases. Coda is more stable, allowing estimates for more pairs that do not have similar focal mechanisms or are not as well recorded. Because reliable source terms are a vital foundation for this effort, we made significant efforts to compare source results from coda and direct phases. Fisk and Phillips (2010) provided detailed comparisons, and to published results that used local data, highlighting the dependence on station coverage and the benefits of using multiple, independent measurements. Agreement of the coda and direct-phase results help to validate the source terms. Discrepancies flag various (e.g., data quality) problems. We have established a large set of events with consistent moments and corner frequencies from coda and direct phases, corresponding to an extensive set of paths in Eurasia.

We have since been focusing on fitting source-corrected spectra to estimate the frequency dependence of Q for fixed paths. This is an orthogonal approach to amplitude tomography analysis at LANL, which estimates the path dependence of Q for fixed frequency bands. Comparison of these independent results corroborate Q estimates for many paths, generally in the interior of the tomography grid, with good station coverage. There are also some large discrepancies, particularly in the γ estimates, that demonstrate the need for further improvements. The Q spectral fitting results can be improved for stations with strong site effects by using independent coda site terms, as shown for KMI. The tomography results can also be improved, especially at the edges of the grid where there are few or no crossing ray paths, and by improving data quality criteria, particularly for higher frequency bands.

Dr. Phillips has been incorporating my source terms directly in his tomography analysis. We plan to evaluate improvements by including these source constraints. In addition to extending this analysis of Lg to remaining paths, we plan to continue processing and fitting source-corrected spectra of Sn, Pg, and Pn.

ACKNOWLEDGMENTS

Seismic data from IRIS were used in this study.

REFERENCES

Brune, J. N. (1970). Tectonic stress and the spectra of seismic shear waves from earthquakes, *J. Geophys. Res.* 75: 4997-5009.

Fisk, M. D., G. D. McCartor, and S. R. Taylor (2008). Robust Magnitude, Distance, and Path-Specific Corrections for Regional Seismic Phases by Constrained Inversion and Enhanced Kriging Methods, ATK/NCR-0608-501, Final Report.

Fisk, M. D. and W. S. Phillips (2010). A Stepwise, Iterative Procedure to Constrain Stress Drop, Regional Attenuation Models, and Site Effects, in *Proceedings of the 2010 Monitoring Research Review: Ground-Based Nuclear Explosion Monitoring Technologies,* LA-UR-10-05578, Vol. 1, pp. 57-66.

Mayeda, K. M., A. Hofstetter, J. L. O'Boyle, and W. R. Walter (2003). Stable and Transportable Regional Magnitudes Based on Coda-Derived Moment-Rate Spectra, *Bull. Seism. Soc. Am.* 93: 224-239.

Mayeda, K. M., L. Malagnini, and W. R. Walter (2007). A new spectral ratio method using narrow band coda envelopes: evidence for non-self-similarity in the Hector Mine sequence, *Geophys. Res. Lett.* 34: L11303.

Phillips, W. S., R. J. Stead, G. E. Randall, H. E. Hartse and K. Mayeda (2008). Source effects from broad area network calibration of regional distance coda waves, in *Scattering of Short Period Waves in the Heterogeneous Earth*, H. Sato and M.C. Fehler, Editors.

Schaff, D. P. and P. G. Richards (2004). Repeating seismic events in China, *Science* 303: 1176-1178.

Sereno T. J., S. R. Bratt and T. C. Bache (1988). Simultaneous inversion of regional wave spectra for attenuation and seismic moment in Scandinavia, *J. Geophys. Res.* 93: 2019-2035.

Taylor, S. R., and H. E. Hartse (1998). A procedure for estimation of source and propagation amplitude corrections for regional seismic discriminants, *J. Geophys. Res.* 103: 2781-2789.

Taylor, S. R., A. A. Velasco, H. E. Hartse, W. S. Phillips, W. R. Walter, and A. J. Rodgers (2002). Amplitude corrections for regional seismic discriminants, *Pure and Appl. Geophys.* 159: 623-650.